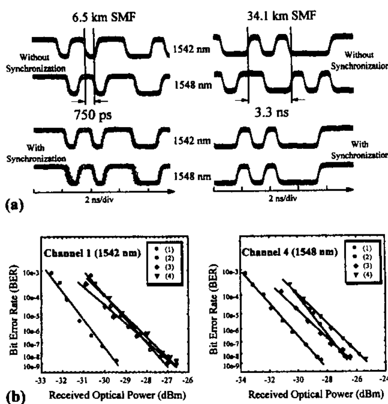

CTuT1 Fig. 3. (a) Received unsynchronized and synchronized 1 Gbit/s bit streams after transmission through 6.5 km and 34.1 km of fiber for the 1542 nm and 1548 nm wavelength channels. (b) BER measurements for (1) baseline with max. data voltage swing, (2) baseline with data and SCM pilot tones transmitted together, (3) after 6.5 km SMF and (4) after 34.1 km SMF transmission.

the fine synchronization in the outer channels of 3/8 of a bit time. The lower frequency tones provide coarse synchronization over several bit times in the electronic domain by shifting the incoming data over several bits according to the phase difference of the two tones.

Figure 2 shows the setup of the RF detection module. After high pass filtering the signal from the two outer wavelengths, the subcarrier is extracted and used for downconverting the pilot tones. These tones generate two quadrature signals that are used to detect their phase differential and accurately determine the time skew.

We simultaneously transmit 1-Gbit/s NRZ data and the SCM pilot tones in the two outer wavelength channels located at 1542 nm and 1548 nm. The unsynchronized and synchronized received channels are shown in Fig. 3(a) after propagation through 6.5 and 34.1 km of fiber that provide, respectively, a skew of 750 ps (i.e., fine) and 3.3 ns (i.e., fine and coarse). In Fig. 3(b), the bit error rate (BER) curves show <2-dB power penalty.

We emphasize that: (i) the time stability of the pilot tones is typically 1 part-per-million, thereby enabling robust synchronization for relatively long data streams, and (ii) this RF-based technique can easily scale to much higher data rates.

1. G.L. Lui, H.H. Tan, IEEE Trans. on Communications 3, 227–237, (1986).
2. M.L. Loeb, G.R. Stilwell, IEEE J. Lightwave Technol. 8, 1306–1311 (1988).
3. L. Bergman, J. Morookian, C. Yeh, IEEE J. Lightwave Technol. 9, 1577–1582 (1998).
4. T. Sangsiri, S. Havstad, C. Kim, A.E. Willner, in OFC'98, 221–222 (1998).
5. C.-L. Lu, D.J.M. Sabido IX, P. Poggiolini, R.T. Hofmeister, L.G. Kazovsky, IEEE Photon. Technol. Lett. 5, 555–557 (1995).

CTuT2 **4:45 pm**

Self-assembled micro-scanner fabricated by surface-micromachining technology

G.D. Su, M.C. Wu, *UCLA, Electrical Engineering Department, 66-147D Engineering IV, 405 Hilgard Avenue, Los Angeles, California 90095-1594 USA; E-mail: wu@icsl.ucla.edu*

Optical scanners are used in a wide variety of applications such as printing, quality inspection, confocal microscopy, data storage, precision pattern generation, display, and medical imaging. Scanning micromirrors fabricated using the micromachining technology is very attractive because of smaller size, lighter mass, and lower power consumption. Earlier works on micromachined scanning mirrors have been realized by either bulk or surface micromachining technology.[1–3] Surface-micromachined optical scanners are particularly interesting because they can be integrated with other micro-mechanical and/or optoelectronic devices. However, the scan angles of current surface-micromachined scanners are limited by the displacement of in-plane actuators such as comb drive[1] and bimorph micro-actuators.[2] Torsion mirrors with angular gap closing actuators, on the other hand, have larger rotation angles.[4] In this paper, we report on the performance of an out-of-plane tilt torsion mirror that can be self-assembled by the integrated scratch drive actuator (SDA).[5] This device is compact, lightweight, and can be mass-produced at potentially very low cost.

The scanning electron micrograph (SEM) of the tilt torsion mirror is shown in Fig. 1. The scanner consists of a torsion mirror, a polysilicon frame and, a SDA actuator. The torsion mirror is suspended by a polysilicon frame that is self-assembled by the integrated SDA. It is designed to rotate up to 12° towards the substrate before it is pulled in by the electrostatic force. The 600-nm-thick low-stress LPCVD silicon nitride layer is deposited on the substrate as an electrical isolation layer. One advantage of this design is that the substrate can be used as the electrode to increase reliability, as compared with the previous design.[4] The principle of operation is illustrated in Fig. 2. The micromirror, originally lying on the substrate after fabrication, is assembled by applying voltage pulses to the SDA actuator. Then, the actuator moves forward to push up the polysilicon frame that is connected to the micromirror. Therefore, the initial angle between the mirror and the substrate can be controlled by manipulating the traveling distance of the SDA. The mirror is 300 μm wide, 250 μm tall and 1.5 μm thick. The torsion beam is 912 μm long, 2 μm wide and 1.5 μm thick. The scan angle versus the DC bias voltage is plotted in Fig. 3(a). The torsion mirror has a maximum pull-in angle of 12° at the voltage of 110 V. The pull-in voltage depends on the initial angle of the polysilicon frame, as shown in Fig. 3(b). The resonant frequency is measured to be 0.5 kHz. The torsion mirror can operate in either small-signal or large-signal regime. For small-signal operation, the mirror scans up to 12° (corresponding to an optical scan angle of 24°) and can be used as scanners. The calculated maximum number of resolvable spots for this scanner is 200. When the peak bias voltage exceeds pull-in voltage, the mirror operates in bistable mode and can be used as an optical switch or chopper.

In summary, a novel out-of-plane self-

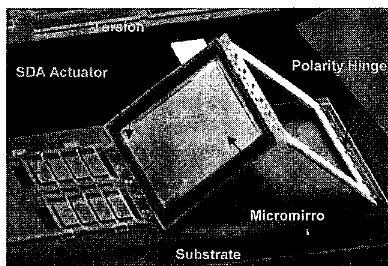

CTuT2 Fig. 1. The scanning electron micrograph of the self-assembled 1D scanner.

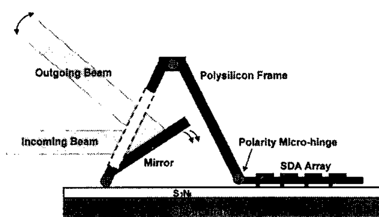

CTuT2 Fig. 2. Schematic diagram illustrating the operation of the scanning torsion mirror.

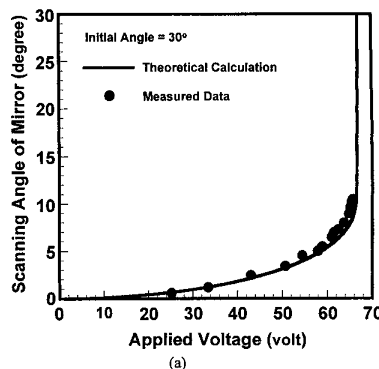

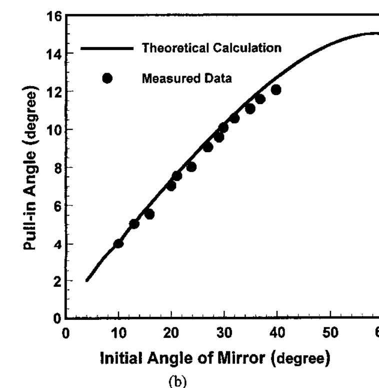

CTuT2 Fig. 3. (a) Scan angle versus applied DC bias voltage, and (b) the pull-in angle versus initial angle of the torsion mirror.

assembled tilt torsion mirror made by surface-micromachining technology has been successfully demonstrated. An optical scan range of 24° and a resonant frequency of 0.5 kHz have been achieved. Its applications include optical scanners, switches, and on-chip optical choppers for monolithic micro-optical instruments.

1. M.-H. Kiang, O. Solgaard, R.S. Muller and K.Y. Lau, "High-Precision Silicon Micromachined Micromirrors for Laser Beam-Scanning and Positioning," Solid-State Sensor and Actuator Workshop, Late News Paper, June 2–6, 1996, Hilton Head Island, SC.
2. M.E. Motamedi, S. Park, A. Wang, M. Dadkhah, A.P. Andrews, H.O. Marcy, M. Khoshnevisan, A.E. Chiou, R.J. Huhn, C.F. Sell, J.G. Smits, "Development of micro-electro-mechanical optical scanner," Optical Engineering,vol. 36, (no. 5), SPIE, May 1997. p. 1346–53.
3. M. Ikeda, H. Goto, H. Totani, M. Sakata, T. Yada, "Two-dimensional miniature optical scanning sensor with silicon micromachined scanning mirror," Proceedings of the SPIE-The International Society for Optical Engineering, vol. 3008, (Miniaturized Systems with Micro-Optics and Micromechanics II, San Jose, CA, USA, 10–12 Feb. 1997.) SPIE-Int. Soc. Opt. Eng, 1997. p. 111–22.
4. G.D. Su, S.S. Lee and M.C. Wu, "Out-of-plane vertical torsion mirror for optical scanner and chopper applications," Proceeding of CLEO 98, San Francisco, CA, USA, p. 479–480 (May 1998).
5. T. Akiyama and H. Fujita, IEEE Micro Electro Mechanical System Workshop, Amsterdam, the Netherlands, Jan. 29–Feb. 2, 1995.

CTuT3 **5:00 pm**

Polarization-independent waveguide modulators using 1.57 m-strained InGaAs/InGaAsP quantum wells

Robert E. Bartolo, S.S. Saini, T. Ren, Y. Zhu, M. Dagenais, H. Shen,* J. Pamulapati,* W. Zhou,* O. King,** F.G. Johnson,** *Department of Electrical Engineering, University of Maryland, College Park, Maryland 20742 USA; E-mail: rbartolo@eng.umd.edu*

The performance of multiple quantum well (MQW) electroabsorption (EA) waveguide modulators based on the Quantum Confined Stark Effect (QCSE) shows considerable promise due to the low drive voltage, enhanced excitonic absorption, and high-speed operation.[1] Most fiber optical communication systems do not preserve the signal polarization, so it is essential that MQW devices that are used operate independent of the input polarization. Since the transverse magnetic (TM) absorption is due to the first light-hole (LH1) subband to electron transition and transverse electric (TE) absorption is mainly from the first heavy-hole (HH1) subband to electron transition, tensile strain has been used in MQW devices to restore the degeneracy of the two

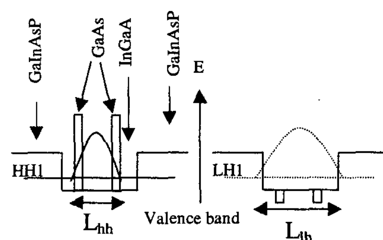

CTuT3 Fig. 1. Valence band diagrams, as well as wave functions for the heavy-hole and light-hole subbands.

levels. However, this degeneracy is destroyed upon application of a reverse bias since the shift in the ground state energy due to the QCSE is proportional to the effective mass m^2

$$Cme^2L^4F^2/h^2, \quad (1)$$

where L is the width of the QW, and F is the applied electric field. To first order, it can be seen from Eq. 1 that an equivalent Stark shift for both the HH1 and LH1 can be obtained provided the product of the effective mass and the fourth power of the well width are designed to be equal. Our approach[3] uses a unique quantum well design that incorporates two thin highly tensile strained GaAs-strain layers in order to provide separate confinement, and effective well widths denoted L_{lh} and L_{hh}, for the LH1 and HH1 wavefunctions respectively, as illustrated in Fig. 1. This design maintains the degeneracy of the LH1 and HH1 energy levels, for polarization independent transmission, for potentially larger values of the electric field as compared to other approaches.

The QW design consisted of a five period, 90 Å $In_{0.53}Ga_{0.47}As$ quantum well and 100 Å $Ga_{0.27}In_{0.73}As_{0.57}P_{0.43}$ barrier. The peak in the PL spectrum was at 1.570 m for both TE and TM. The 3 monolayer GaAs-strain layers are located 20 Å from the $In_{0.53}Ga_{0.47}As$ quantum well edge as illustrated in Fig. 1. It was necessary to etch past the active region in order to ensure equal confinement for both TE and TM. A methane based reactive ion etching process was used to define 2.3 m wide ridges deep-etched to a total depth of 2.9 m, 0.7 m past the active region.

The transmission measurements as a function of reverse bias were performed using a tunable external cavity laser over the wavelength range 1.610–1.630 m as shown Fig. 2. The solid (open) symbols are for TE (TM) respectively. At zero volts reverse bias, the difference between TE and TM is within 1 dB over a 20 nm range. A 3 dB difference in the polarization dependence is maintained over a 2 V range. The on/off ratio was as large as 18 dB for 2 V at 1630 nm. The deep etch process was essential to achieving polarization independence since for narrow ridge devices, etched only to a depth of 1.2 m, the TE transmission was *smaller* than TM by 4–6 dB.

U.S. Army Research Laboratory, Adelphi, Maryland 20783 USA; E-mail: Paul_Shen@emh3.arl.mil

**Laboratory for Physical Sciences, College Park, Maryland 20740 USA; E-mail: KING@lps.umd.edu*

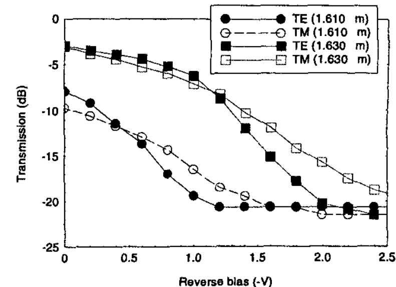

CTuT3 Fig. 2. Transmission as a function of reverse bias for =1.610–1.630 m for a 300 m long narrow-ridge (2.3 m) deep-etch single mode waveguide.

1. F. Devaux, S. Chelles, A. Ougazzaden, A. Mircea, and J.C. Harmand, "Electroabsorption modulators for high-bit-rate optical communications: a comparison of strained InGaAs/InAlAs and InGaAsP/InGaAsP MQW," Semicond. Sci. Technol., vol 10, pp. 887–901, 1995, and references therein.
2. G. Bastard, E.E. Mendez, L.L. Chang, and L. Esaki, "Variational calculations on a quantum well in an electric field," Phys. Rev. B, vol. 28, pp. 3241–3245, 1983.
3. H. Shen, J. Pamulapati, W. Zhou, M. Dutta, and F.G. Johnson, "Bias independent heavy-and light-hole degeneracy in InGaAs/InGaAsP quantum wells," Appl. Phys. Lett., vol. 72, pp. 683–685, 1998.

CTuT4 **5:15 pm**

Annealing of low-temperature grown semiconductors: material optimization for ultrafast all-optical gating

M. Haiml, U. Siegner, F. Morier-Genoud, U. Keller, M. Luysberg,* P. Specht,** E.R. Weber,** *Swiss Federal Institute of Technology Zurich, Institute of Quantum Electronics, ETH Hönggerberg HPT, CH-8093 Zurich, Switzerland; E-mail: haiml@iqe.phys.ethz.ch*

Ultrafast all-optical gating with compact semiconductor devices[1,2] requires materials with high absorption modulation, sub-picosecond response times, and low absorption in the fully saturated state (low nonsaturable losses). While the time response in low-temperature grown (LT) semiconductors, as e.g. GaAs, has been intensively investigated,[3] only limited information is available about the strength of the modulation. For the first time, we correlate the time response with the strength of the modulation in as-grown and annealed LT-GaAs. The modulation is very weak in as-grown LT-GaAs with sub-picosecond response times. We demonstrate that annealing substantially increases the modulation and preserves a fast, sub-picosecond response, yielding a superior material for ultrafast all-optical gating. A qualitative model is presented which relates the material properties to the defect structure and the defect-related optical transitions in LT-GaAs. Based on this model, for the first time, guidelines are obtained for controlled defect